NRC Publications Archive
Archives des publications du CNRC

Thermo-physical modelling of track width during laser polishing of H13 tool steel

Mohajerani, Shirzad; Miller, Joshua D.; Tutunea-Fatan, O. Remus; Bordatchev, Evgueni V.

This publication could be one of several versions: author's original, accepted manuscript or the publisher's version. / La version de cette publication peut être l'une des suivantes : la version prépublication de l'auteur, la version acceptée du manuscrit ou la version de l'éditeur.

For the publisher's version, please access the DOI link below./ Pour consulter la version de l'éditeur, utilisez le lien DOI ci-dessous.

Publisher's version / Version de l'éditeur:

https://doi.org/10.1016/j.promfg.2017.07.026
Procedia Manufacturing, 10, pp. 708-719, 2017-07-07

National Research Council Canada   Conseil national de recherches Canada

Canada

45th SME North American Manufacturing Research Conference, NAMRC 45, LA, USA

Thermo-Physical Modelling of Track Width During Laser Polishing of H13 Tool Steel

Shirzad Mohajerani[a], Joshua D. Miller[a], O. Remus Tutunea-Fatan[a], Evgueni V. Bordatchev[b]*

[a]Mechanical and Materials Engineering, Western University, London, Ontario, Canada
[b]National Research Council of Canada, London, Ontario, Canada

Abstract

A three-dimensional CFD model has been developed to predict track width during laser polishing (LP) of H13 tool steel. The developed model incorporates several different mechanisms for heat transfer such as conduction, convection, and radiation as well as temperature dependencies for relevant material properties. Experimental calibration was carried out to obtain adequate absorptivity value. After performing the mesh-sensitivity assessment, simulation results have been validated against experimental data. The relatively low errors obtained suggest that the developed model is capable to accurately describe the effect of process parameters on molten pool dimensions and/or geometry.

Keywords: : Laser polishing; thermo-physical model; numerical simulation; experimental calibration

1. Introduction

The majority of the manufacturing processes cannot be used as primary means to generate acceptable surface quality. For instance, while the roughness of the forged parts varies between 3.2 µm and 12.5 µm, milling will typically yield surfaces with R_a between 0.8 µm and 6.3 µm [1]. However, for many applications, these values are

---

* Corresponding author. Tel.: +1-519-430-7107; fax: +1-519-430-7064.
  E-mail address: evgueni.bordatchev@nrc-cnrc.gc.ca

well above the acceptable levels of quality such that secondary polishing processes are required to further improve the roughness of the surface.

Among them, laser polishing (LP) represents a contactless manufacturing option that continue to receive a constant attention during the past decade, particularly since it was shown that it can produce surface quality improvements of up to 90-95% [2]. Moreover, LP enables the possibility of selective polishing for small areas (< 0.1 mm^2) that can be used to prevent problems like edge rounding [3]. By accounting for workpiece material, initial roughness and laser parameters, it was determined that LP process can be run with speeds of up to 3 s/cm^2 and that is 600 times faster than the conventional manual polishing techniques that is still widely used by the mold and die industry [4].

The surveyed literature suggests that LP can be successfully used to enhance the surface quality of a wide range of metallic [2] and nonmetallic materials [4, 5]. However, uncontrollable/unknown mechanisms occurring during melting and solidification phases of LP can introduce a broad variety of defects such as undercuts, ripples, bulges, martensite needles and step structures which in turn will decrease the overall surface quality of the polished surface [6]. Evidently, a deeper understanding of the interactions between various LP parameters might be able to prevent the formation of such unwanted structures but so far, LP process was primarily investigated by means of costly and time consuming trial-and-error experiments.

The traditional complement of the experimental work is constituted by the theoretical analysis that – when adequately performed – could provide important insightful information regarding the thermo-physical mechanisms underlying the LP process. However, with the exception of several analytical or semi-analytical studies [7-9], the vast majority of non-experimental works reported so far have relied on numerical methods, most likely due to the high complexity and/or nonlinearity of the phenomena involved. For instance, the one-dimensional unsteady model proposed in [10] was capable to determine the energy density required for melting of the silicon carbide during LP. Along the same lines, a 1D unsteady model was also devised in [11] in order to determine the melting depth. The inherent simplifying assumptions of the model were related to a uniform laser distribution energy as well as a dominant conduction mode for heat transfer. By contrast, a 2D modified fixed domain method in conjunction with Stephan boundary equation has been used in [12] to trace the liquid-solid boundary in a molten pool during polishing of 304 stainless steel and melt depth has been predicted by an enthalpy-based model solved through the CFD technique in [13, 14].

Pre- and post-polished surface geometry was also one of the points of interest for some of the past simulation works. In this context, the decomposition of the initial surface geometry into different spatial frequency components was used in [15] to predict the post-polished surface topography and a number of later studies [16-19] have reinforced the idea that critical frequency represents to date, one of the most important theoretical advancements in the field of LP. All previously-reported simulations imply that the accuracy of the heat transfer simulation can significantly influence the accuracy of the modeling result.

However, to the best of our knowledge, no prior attempts were made to analyze the width of the polished track along a LP line as a measurable process outcome. As such, the aim of the present work was to develop a numerical model capable to predict the width of the polished line by reducing the number of simplifying assumptions that would inevitably lead to less accurate predictions. In the current implementation, material absorptivity (*i.e.*, the capacity of the workpiece material to partially absorb the incident laser energy) will be specified throughout experimental calibration as it plays a prominent role on the overall thermodynamic balance of the process. It is also important to note here that the width of the laser polished track has important implications on both the quality of the polished surface as well as the overall tool path planning strategy to be adopted.

2. Thermo-physical processes underlying laser polishing

Undoubtedly, a good understanding of the thermo-physical processes and laser/material properties/interactions constitute some of the key ingredients of reliable and accurate LP simulations. In this context, it can be stated that when laser irradiates the surface a certain fraction of its energy will be absorbed into the workpiece while the rest will be reflected and thereby affect the surrounding environment. The fraction of absorbed energy, defined by absorptivity, depends on the surface properties of the workpiece as well as the electromagnetic wave properties of laser beam [20].

Following this logic, it can be inferred that the laser energy that is absorbed by the workpiece will be converted

to heat and subsequently propagate to the core of the material predominantly through a conduction mechanism. It is well accepted that the increased atomic oscillations caused by a rapid rise in the workpiece material temperature will result in their lattice breakoff followed by the onset of the melting. However, the amount of energy delivered should be adjusted precisely to control the depth of the melting while avoiding material vaporization - also known as laser ablation that occurs in laser machining, cutting, drilling, texturing, etc.. Therefore, a narrow working window exists in terms of absorbed laser fluence that has to be chosen in such a way that determines only melting while heating and ablation will occur beneath and above it, respectively [15].

The superficial layer of the workpiece material redistributes under the action of laser energy (and possibly gravitational forces) by flowing from peak to valleys. The combined balance between capillary pressure, gravity and viscosity yields a phenomenon known as Surface Shallow Melting (SSM) [8]. The delivery of additional heat results in a gradually evolving liquid boundary in the bulk material that constitutes a prerequisite for the formation of the molten pool. In this latter mechanism – typically known as Surface Over-Melting (SOM) [8] – the surface tension caused by the temperature gradient tends to counteract the action of the viscous forces and leads to the formation of the molten pool flow regime. If the surface tension gradient prevails the viscous force in the molten pool, the Marangoni flow (thermocapillary regime) will dominate the fluid flow [18].

In case of pulsed lasers, the solidification of the molten material begins when the pulsed laser radiation ceases. Prior to that, superficial material is capable to relocate during the time interval elapsed between the commencement of melting and the completion of solidification. This short duration can be controlled by adjusting the laser scanning speed and/or pulse duration. It is also important to remember that in addition to the aforementioned heat conduction into the workpiece, the other thermo-physical processes associated with LP include convection and radiation into the surrounding air. However, the dynamic/short-timed nature of laser energy delivery into the workpiece suggests that convection would be of a rather secondary importance in the overall balance of LP, such that it will assumed further that conduction and radiation are in fact the primary heat transfer mechanisms affecting the final outcome of the polishing process that would in turn determine the post-polished surface topography.

When it comes to conduction and radiation, different material properties such as density, specific heat capacity, conductivity and viscosity play a significant role on the overall outcome of LP. However, unlike LP process parameters that can be continuously adjusted in order to obtain "the best" final surface roughness, these material properties can be – at most – precisely known as a function of the temperature of the material. Without an accurate understanding of this fundamental temperature dependence, most of the numerical analyses of the LP are prone to be – partly and/or largely – erroneous.

3. Numerical modelling methodology

A three-dimensional unsteady heat transfer CFD model has been developed in ANSYS Fluent with the aim to numerically analyze the continuous wave (CW) LP of H13 tool steel. The temperature distribution across the workpiece was obtained by means of a finite volume model allowing the calculation of width and depth of the molten pool. The basic assumptions associated with this model were: i) material isotropy and homogeneity; ii) the flow of the material during melting and solidification was neglected such that the geometry of the domain does not change during LP; iii) no chemical reaction occurs during LP due to the protective argon shielding; and iv) the CW laser beam characterized by a Gaussian distribution is assimilated with a surface source acting on the top surface of the workpiece.

3.1. Mesh geometry

To perform the intended numerical analysis, a rectangular cuboid domain sized at 8×4×1.5 mm (length×width×thickness) was modeled in accordance with the workpiece to be used during the calibration experiments. The workpiece was initially meshed with 320×120×20 hexahedral elements to a total of 768,000 over the entire domain. As the laser traverses along a straight line across the top surface, a mesh refining technique was used to further decrease the size of the elements located along the intended laser polishing path (Figure 1).
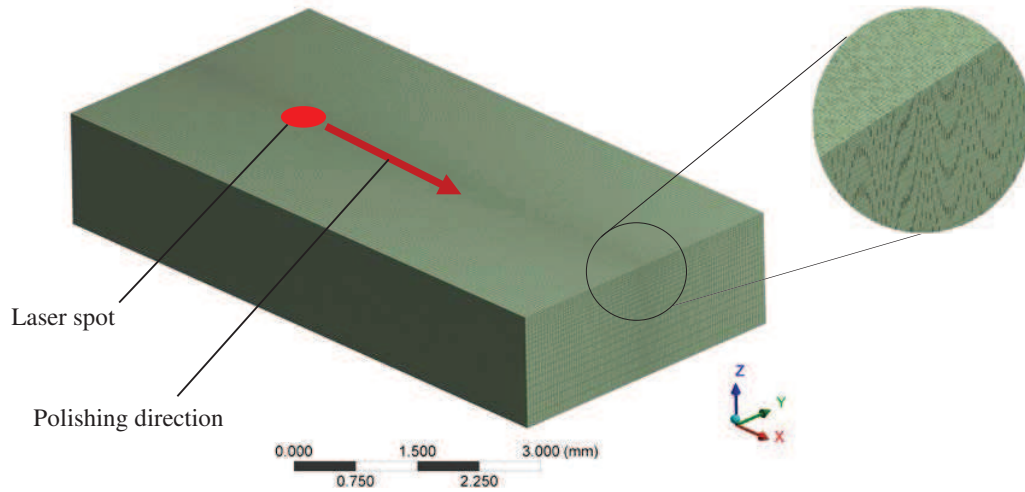
Fig. 1. Meshed geometry of the workpiece.

3.2. Heat transfer mechanisms

The temperature distribution throughout the 3D domain was calculated by means of the traditional energy transport equation [21]:

$$\frac{\partial}{\partial t}(\rho H) = \nabla.(k\nabla T), \tag{1}$$

in which ρ, k and T are the density, conductivity and temperature of the workpiece, respectively while H represents the total enthalpy defined by [21]:

$$H = h_{ref} + \int_{T_{ref}}^{T} c_p dT \tag{2}$$

Here, c_p represents the specific heat capacity in constant pressure and h_{ref} and T_{ref} are the reference enthalpy and temperature, respectively.

3.3. Boundary conditions

To account for the laser radiation and convection with the surrounding gaseous environment, boundary conditions were set as described further.

Fourier's law was used to account for the absorption of laser heat flux on top of the workpiece surface:

$$k\nabla T = q'' \tag{3}$$

in which q'' is the absorbed laser flux as defined by:

$$q'' = AP_{x,y} \tag{4}$$

where $P_{x,y}$ is the incident heat flux and A is the absorptivity to be experimentally determined through calibration as detailed in the upcoming Section 4. The incident heat flux travels along the polished line with the same velocity as that of the incident laser beam.

The incident laser flux is characterized by a Gaussian distribution as described by [14]:

$$P_{x,y} = I_0 \exp\left(-\frac{2r^2}{w^2}\right) \tag{5}$$

where r is the radial position, and w (Gaussian beam radius) represents the radius at which the laser intensity is $1/e^2$ ($= 0.135$) of its peak value at the center of the beam. Peak energy density (I_0) is given by:

$$I_0 = \frac{2P}{w^2\pi} \tag{6}$$

where P is the total laser power. In this model, Gaussian laser intensity is applied on a radius ranging between -*1.51743w* and *1.51743w* where laser intensity ranges between *0.01 I_0* and *I_0*. For the remainder of the workpiece surfaces, only the convection with surrounding gas was considered:

$$k\nabla T = h(T_\infty - T_s) \tag{7}$$

in which h is the convection heat transfer coefficient, and T_s and T_∞ are the surface and surrounding gas temperature. To consider heat flux emitted by the top surface to the surrounding area, radiation equation [22] was used for the top surface of the workpiece:

$$q''_{rad} = \varepsilon\sigma(T_s^4 - T_\infty^4) \tag{8}$$

where q''_{rad} is the emitted heat flux, $\varepsilon \in [0,1]$ represent the surface emissivity, while $\sigma = 5.56 \times 10^{-8}$ W/m²K⁴ is the Stefan-Boltzman constant. The above-mentioned boundary conditions were introduced in the model by means of the user-defined functions (UDF).

All the aforementioned boundary conditions were introduced into the model by means of the UDF written in C programming language.

3.4. Temperature-dependent material properties

To be able to complete the model, the thermo-physical material properties of H13 tool steel have to be specified. Among them, material density (ρ), conductivity (k), specific heat capacity (c_p), absorptivity (A) and emissivity (ε) are regarded as the most important ones and they will be detailed further. Evidently, their precise temperature dependence represents one of the key factors with a direct effect on the outcome of the modeling problem at hand.

Similar to the majority of metallic alloys, H13 tool steel is not characterized by a unique "melting temperature" since the melting process occurs between solidus (T_{sol}) and liquidous (T_{liq}) temperatures. According to the reference [23], these two temperatures are 1315°C and 1454°C, respectively.

To account for the latent heat of melting, the specific heat capacity shown in Eq. (2) can be expressed between solidus and liquidous temperature as:

$$c_p' = c_p + \frac{L}{T_{liq} - T_{sol}}, \text{ when } T_{sol} \leq T \leq T_{liq} \tag{9}$$

where c_p' is the corrected heat capacity and $L = 2.8 \times 10^5$ J/kg is the latent heat of fusion for H13 [23]. When accounting for the temperature dependence of the heat capacity [23, 24] as well as that described by Eq. (9), the temperature-dependent variation of heat capacity could be graphically represented as depicted in Figure 2.
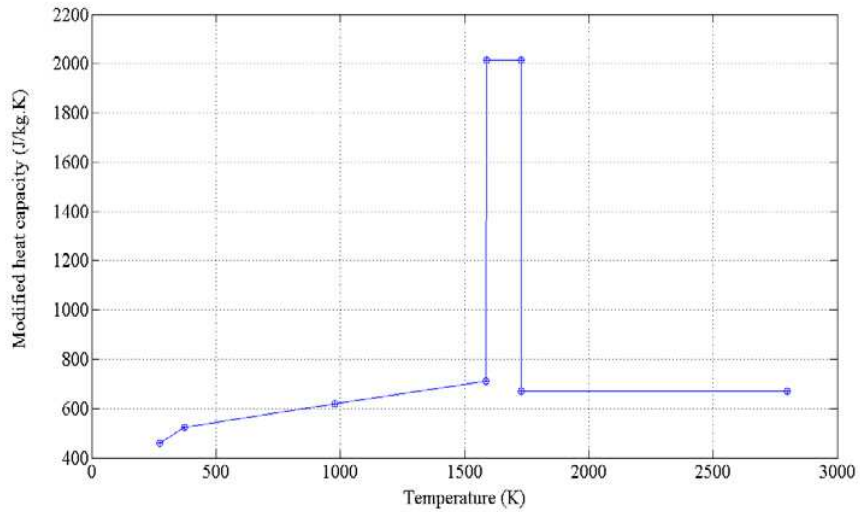
Fig. 2. Temperature-dependent correction of H13 heat capacity

Furthermore, the temperature dependence of material conductivity (k) and density (ρ) that were implemented in the numerical model are graphically represented in Figures 3 and 4, respectively. Both plots were based on the data reported in references [23-26].

Based on reference [27], material emissivity ε was set as 0.5. By contrast, the absorptivity (A) was determined by means of the experimental calibration described in a subsequent section.
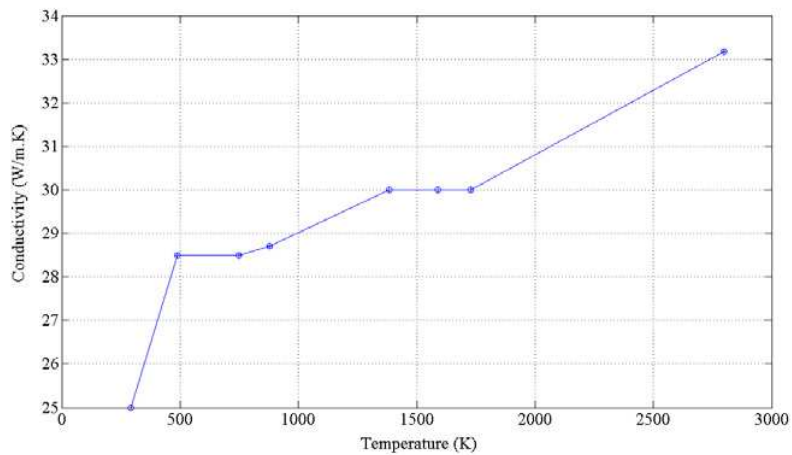

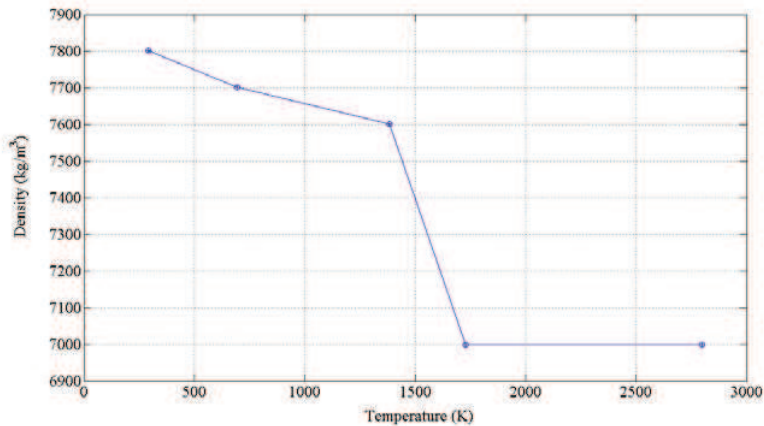Fig. 3. Temperature-dependent conductivity of H13

Fig. 4. Temperature-dependent density of H13

4. Results

When it comes to the validation of the thermo-physical models, many of the past studies have relied on geometry of the molten pool as the matching characteristic between simulation and experimental analyses. In all these cases, a cross section taken through the median plane of the polished track was used to assess the correspondence with the simulation results, either from the perspective of molten pool depth [7], molten pool width [12] or both [13, 18]. However, the quantification of the molten pool characteristics was rather imperfect in a sense that the delimitation between heat-affected zone and bulk material was performed in a rather visual manner. Indentation-based hardness measurements of the different metallographic cross sectional regions are also possible, but – especially in case of low power LP – the relatively large size of the indenter trace could sometimes prevent accurate identifications of the various cross sectional layers.
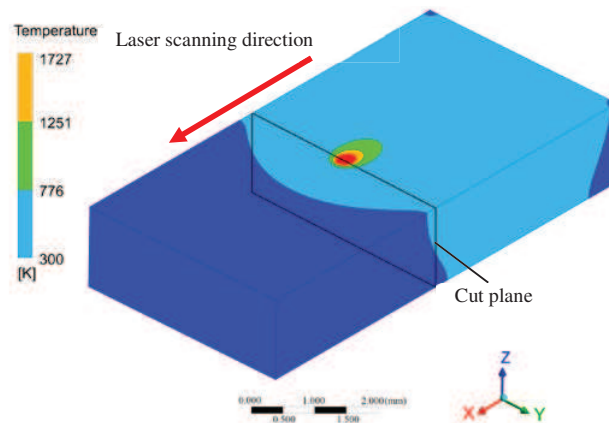

Fig. 5. Sample temperature field 45 ms after the start of the laser beam motion

In contrast with all other prior attempts, the current study will attempt to establish modelling-experimental correlations by means of the polished track whose width can be accurately measured by means of optical instruments. From a simulation perspective, the distribution of the temperature throughout the entire domain can be determined at every time step such that molten pool dimensions could be simply assimilated with the regions in

which the temperature exceeds the liquidous temperature. As an illustration of this concept, Figure 5 shows a sample snapshot of the distribution of the temperature at the surface of the workpiece as computed at 45 ms after the start of the laser motion along the programmed polishing line.

When a transversal cross section is cut through the plane shown in Figure 5, an in-depth depiction of the various temperature-dependent regions can be extracted (Figure 6).
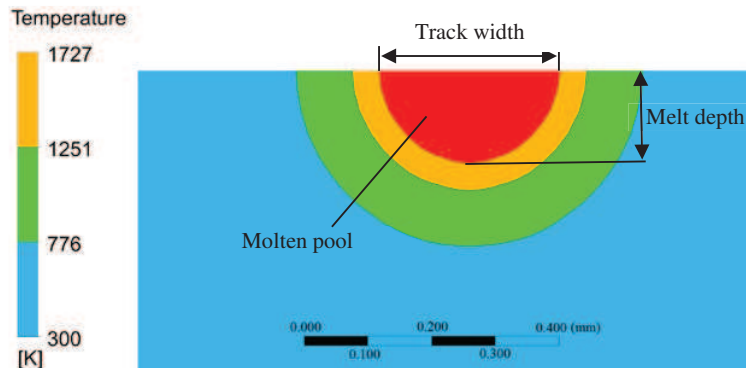

Fig. 6. Sample molten pool geometry as seen in a transversal cut plane

The red colored domain - characterized by temperatures in excess of 1727 K – can be assimilated with molten pool as developed during laser polishing. As implied above, direct comparisons between numerically and experimentally determined track width can be used to calibrate the intended thermo-physical model to be then used in a process-behavior predictive manner.

4.1. Experimental calibration of the model

The line polishing experiments used for calibration were conducted on a dual PC setup for laser polishing. One PC was used to control the Aerotech motion control system relying on NView software to coarsely position the H13 workpiece in the correct location within the workspace envelope of the three-axis stage. The second PC was used to control the laser scan head that is responsible for the motion of the laser beam. Without going into too many unnecessary details, it will be briefly stated here that the relatively large inertia associated with an electromechanical system - such is the Aerotech stage – can be counteracted by means of a fast speed optical system such as the laser scanner.

The experimental setup also encompasses a laser with a wavelength of 1070 nm whose beam is delivered to the laser head via a fiber optic cable that is operated in the continuous wave (CW) mode. A 100 mm focal lens is used to concentrate the beam onto the sample that is also placed in a containment chamber that is continuously fed with inert argon gas pumped at 50 cubic feet per hour (CFH). The experiments were conducted in sets differentiated by different laser power levels. The scanner control software is capable to generate polishing lines at different scanning speeds. As an illustration of the typical experimental result, Figure 7a depicts polished lines that were generated at 100 W and 150 W, each running at three different scanning speeds. For each of the polished lines, the track width has been measured by means of a Veeco Wyko NT 1100 optical profilometer whose typical result is shown in Figure 7b.

By returning to the proposed thermo-physical model, the absorptivity (*A*) in Eq. (4) – defined as the ratio between the absorbed and incident energy – depends on both laser properties (*e.g.*, wavelength) as well as material properties (*e.g.*, surface roughness, temperature or chemical composition) [20].
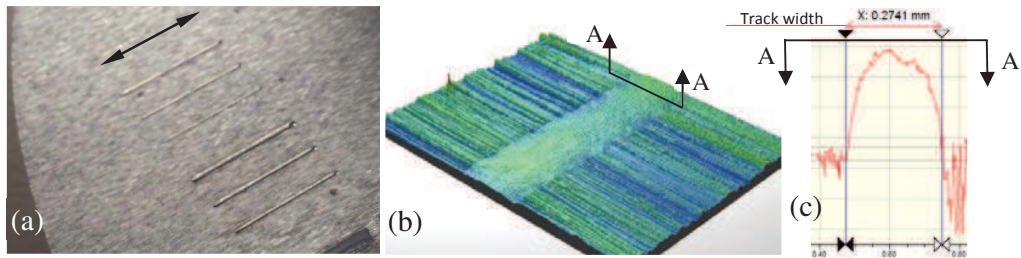
Fig. 7. (a) Representative LPed lines made at 100 W and 150 W; (b) surface topography of a LPed line; (c) LPed line cross-section

Of note, although it is reasonable to believe the absorptivity is a variable (possibly temperature-dependent) material property, the lack of appropriate experimental means has prompted researchers to assume it as a material constant, irrespective of the parameters used to control the LP process. To address this relative gap of knowledge and to more accurately determine absorptivity values as a function of the process parameters, one matching set of simulation and experiment was conducted. For this purpose, LP process parameters were set to 100 W and 50 mm/s, while a theoretical beam diameter ($2w$) was 50 µm at a focal point and laser beam energy profile was having the Gaussian distribution.

Heuristic searches performed through the alteration of the absorptivity value have been used to match the steady state track width yielded from numerical simulations with that measured from the experiment, namely 306.5 µm. Once the relative match was reached, the required absorptivity was determined as being 76.5% for this particular set of LP parameters used.

4.2. Mesh sensitivity study

Prior to any other considerations relying on the developed thermo-physical model, mesh sensitivity studies have to be conducted to demonstrate a relative independence between the results acquired and the size of the mesh used. For this purpose, the model was run with increasing mesh sizes and the profile of the surface temperature was analyzed along the polished line until a minimal difference was noticed between successive runs (Figure 8).
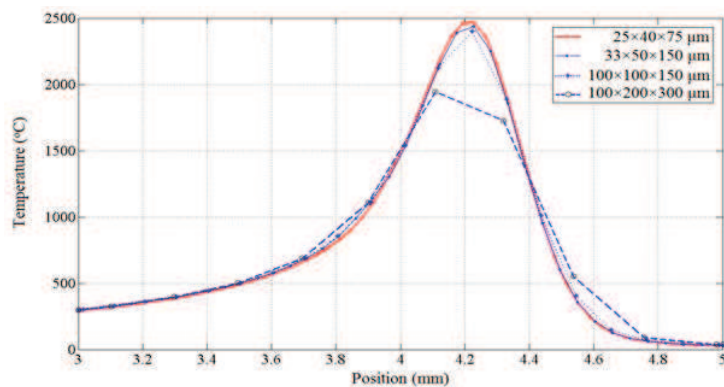

Fig. 8. Mid-track temperature at t = 45 ms

The curves presented in this figure suggest that the models with 33×50×150 µm and 25×40×75 µm element-size are sufficiently close to each other to conclude that at these mesh sizes the model will produce results that are largely independent of the mesh size. As such, the mesh size adopted in Section 3.1 will likely yield sufficiently accurate results.

4.3. Mesh sensitivity study

After the completion of the model calibration and mesh sensitivity assessment, additional comparisons between experimentally and numerically generated steady state LP track widths were performed. For this purpose, LPed lines were made at 100 W and 150 W while varying the scanning speed at 50, 100, and 150 mm/s. The results summarized in Figure 9 suggest that the absorptivity value determined through calibration (Section 4.1) yields relatively accurate matches between simulation and experiment with maximum error values of 4.55% for 100 W and 7.65% for 150 W, respectively.
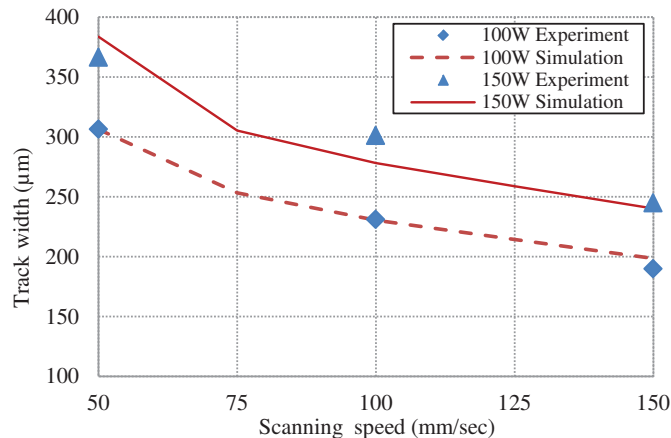

Fig. 9. Simulation and experiment results for steady track width

While past attempts to quantify the absorptivity of the metals [20] have suggested a fairly large range of variation for this particular material property, it seems that a value of 76.5% represents a fair estimation for the line polishing parameters explored within the scope of the present study.

As an interesting observation, it will be outlined here that Figure 9 clearly indicates that at as specific laser energy, the width of the polished track decreases as the scanning speed increases, most likely due to the decreased time available to transfer the energy from the laser heat source to the workpiece. In addition to that, an increased laser power is clearly associated with wider tracks and that is simply because the total amount of energy delivered to the workpiece will increase and in turn, this will lead to larger sizes of the molten pool.

5. Summary and conclusion

To the best of authors' knowledge, the present study represents one of the first attempts made to predict the width of a laser polished line by means of a validated/calibrated thermo-physical model. The developed model can be used to investigate the effect of process parameters – such as laser power and scanning speed – on the track width, a dependent variable with important implications on tool path planning and post-polishing surface quality. While certain similarities exists between the present model and those that were previously used in laser machining, it is believed that the precision of the temperature-dependent material properties (that were derived from data available in the literature) along with the proposed power-dependent material absorbance have contributed to its elevated accuracy.

A three-dimensional thermo-physical model has been developed using CFD software to simulate the heat transfer mechanisms involved that are present during CW LP of H13. The developed model incorporates temperature dependencies for heat capacity, conductivity and density, whereas calibration experiments were conducted to determine appropriate value for the heat absorptivity of the workpiece.

Post-calibration mesh sensitivity studies have shown that the size of the mesh does not influence the accuracy of the results. Finally, additional post-calibration experiments have suggested that the selected value of the absorptivity

enables reasonable matches between LP track widths determined through experimental and numerical techniques such that it can be anticipated that the developed model can be used for further in-depth investigations of the geometry/dimensions of the molten pool.

Acknowledgements

References

[1]   *ASME/ANSI B46.1 surface texture*. 1985, American National standard: New Yorks.

[2]   Bordatchev, E.V., Hafiz, A.M.K., and Tutunea-Fatan, O.R., 2014. Performance of laser polishing in finishing of metallic surfaces. *International Journal of Advanced Manufacturing Technology*, 73(1-4), pp. 35-52.

[3]   Temmler, A., Willenborg, E., and Wissenbach, K. 2012. Laser Polishing. *Proceedings of SPIE*, 8243, paper 82430W, 13 p.

[4]   Willenborg, E., *Polishing with Laser Radiation*, in *Tailored Light 2: Laser Application Technology*, R. Poprawe, Editor. 2011, Springer.

[5]   Vega, F., Armengol, J., Lupon, N., and Laguarta, F., 1999. Study of surface dynamics during laser polishing of glass. *Computer-Controlled Microshaping*, 3822, pp. 92-102.

[6]   Nusser, C., Kumstel, J., Kiedrowski, T., Diatlov, A., and Willenborg, E., 2015. Process- and Material-Induced Surface Structures During Laser Polishing. *Advanced Engineering Materials*, 17(3), pp. 268-277.

[7]   Shen, Z.H., Zhang, S.Y., Lu, J., and Ni, X.W., 2001. Mathematical modeling of laser induced heating and melting in solids. *Optics and Laser Technology*, 33(8), pp. 533-537.

[8]   Ramos, J.A., Bourell, D.L., and Beaman, J.J., 2003. Surface over-melt during laser polishing of Indirect-SLS metal parts. *Rapid Prototyping Technologies*, 758, pp. 53-61.

[9]   Liu, S.Y., Hu, J.D., Yang, Y., Guo, Z.X., and Wang, H.Y., 2005. Microstructure analysis of magnesium alloy melted by laser irradiation. *Applied Surface Science*, 252(5), pp. 1723-1731.

[10]   Dutto, C., Fogarassy, E., and Mathiot, D., 2001. Numerical and experimental analysis of pulsed excimer laser processing of silicon carbide. *Applied Surface Science*, 184(1-4), pp. 362-366.

[11]   Shao, T.M., Hua, A., Tam, H.Y., and Cheung, E.H.M., 2005. An approach to modelling of laser polishing of metals. *Surface & Coatings Technology*, 197(1), pp. 77-84.

[12]   Mai, T.A., Lim, G. C., 2004. Micromelting and its effects on surface topography and properties in laser polishing of stainless steel. *Journal of Laser Applications*, 16(4), pp. 221-228.

[13]   Yilbas, B.S., Shuja, S.Z., Khan, S.M.A., and Aleem, A., 2009. Laser melting of carbide tool surface: Model and experimental studies. *Applied Surface Science*, 255(23), pp. 9396-9403.

[14]   Marimuthu, S., Triantaphyllou, A., Antar, M., Wimpenny, D., Morton, H., and Beard, M., 2015. Laser polishing of selective laser melted components. *International Journal of Machine Tools & Manufacture*, 95, pp. 97-104.

[15]   Perry, T.L., Werschmoeller, D., Li, X.C., Pfefferkorn, F.E., and Duffie, N.A., 2009. The Effect of Laser Pulse Duration and Feed Rate on Pulsed Laser Polishing of Microfabricated Nickel Samples. *Journal of Manufacturing Science and Engineering-Transactions of the Asme*, 131(3).

[16]   Vadali, M., Ma, C., Duffie, N.A., Li, X., and Pfefferkorn, F.E., 2012. Pulsed laser micro polishing: Surface prediction model. *Journal of*

Manufacturing Processes, 14(3), pp. 307-315.

[17] Ukar, E., Lamikiz, A., Martínez, S., Tabernero, I., and Lacalle, L.N.L.d., 2012. Roughness prediction on laser polished surfaces. *Journal of Materials Processing Technology*, 212(6), pp. 1305-1313.

[18] Ma, C., Vadali, M., Duffie, N.A., Pfefferkorn, F.E., and Li, X., 2013. Melt Pool Flow and Surface Evolution During Pulsed Laser Micro Polishing of Ti6Al4V. *Journal of Manufacturing Science and Engineering*, 135(6), pp. 061023-061023.

[19] Wang, Q.H., Morrow, J.D., Ma, C., Duffie, N.A., and Pfefferkorn, F.E., 2015. Surface prediction model for thermocapillary regime pulsed laser micro polishing of metals. *Journal of Manufacturing Processes*, 20, pp. 340-348.

[20] Bergström, D., Kaplan, A., Powell, J., 2003. Mathematical modelling of laser absorption mechanisms in metals: A review. in *the M4PL16 workshop*, Igls, Austria: published by Luleå TU, Sweden.

[21] *ANSYS Fluent Theory Guide*. January 2015.Release 16.

[22] Bergman, T.L., Lavine, A. S., Incropera, F. P., DeWitt, D. P., 2011. *Fundamentals of Heat and Mass Transfer 7th Edition*. United States of America: Wiley.

[23] Lin, Y.J., McHugh, K.M., Park, Y.S., Zhou, Y.Z., and Lavernia, E.J., 2005. Microstructure and mechanical properties of spray-formed H13 steel tooling. *Trends in Materials and Manufacturing Technologies for Transportation Industries and Powder Metallurgy Research and Development in the Transportation Industry*, pp. 45-50.

[24] Benedyk, J.C., 2013. *High Performance Alloys Database,* published by CINDAS LLC, Indiana

[25] Bohler-Uddeholm, 2013. *H13 Tool Steel datasheet. http://www.bucorp.com/media/H13_data_sheet_09032013.pdf*

[26] Wilthan, B., Schutzenhofer, W., and Pottlacher, G., 2015. Thermal Diffusivity and Thermal Conductivity of Five Different Steel Alloys in the Solid and Liquid Phases. *International Journal of Thermophysics*, 36(8), pp. 2259-2272.

[27] OMEGA. *Table of Total Emissivity*. http://www.omega.com/techref/Z-section.html